SUPPORTING INFORMATION

Mechanistic Insight into Peroxydisulfate Reactivity: Oxidation of the *cis,cis*-$[Ru(bpy)_2(OH_2)]_2O^{4+}$ "Blue Dimer"

James K. Hurst,[†] Margo Roemeling,[‡] and Sergei V. Lymar*

[†]Department of Chemistry, Washington State University, Pullman, WA 99164

[‡]Department of Biochemistry and Biophysics, Oregon State University, Corvallis, OR 97331

*Chemistry Department, Brookhaven National Laboratory, Upton, NY 11973

*Corresponding author: e-mail: lymar@bnl.gov; phone: (631) 344-4333; FAX (631) 344-5815

Radii of $S_2O_8^{2-}$ and *cis,cis*-$[(bpy)_2Ru(OH_2)]_2O^{4+}$

The crystallographic shape of $S_2O_8^{2-}$ is that of two overlapping slightly distorted tetrahedral SO_4 units, where the O-O bond is nearly perpendicular to the S-S axis, giving the aspect of a prolate spheroid; the average S-O bond length is 1.48 Å,[1] very nearly the same as the S-O bond length in SO_4^{2-} (1.49 Å). From the equation for the volume of a prolate spheroid ($V = \frac{4\pi}{3}a^2b$, where a and b are the minor and major semi-axes) with a = 1.48 Å and $b = 2a$, an equivalent radius of 1.9 Å is calculated for $S_2O_8^{2-}$. The crystallographic shape of *cis,cis*-$[(bpy)_2Ru(OH_2)]_2O^{4+}$ is that of a distorted hemisphere, where the face containing the *cis*-coordinated water molecules is nearly planar. From the reported crystallographic bond lengths, radii defined by the pyridine units *cis* and *trans* to the nearly linear Ru-O-Ru bond are a = 5.9 Å and b = 8.0 Å, respectively.[2] The corresponding volume, calculated as one-half that of a prolate spheroid, is 583 $Å^3$, giving an equivalent radius of 5.2 Å.

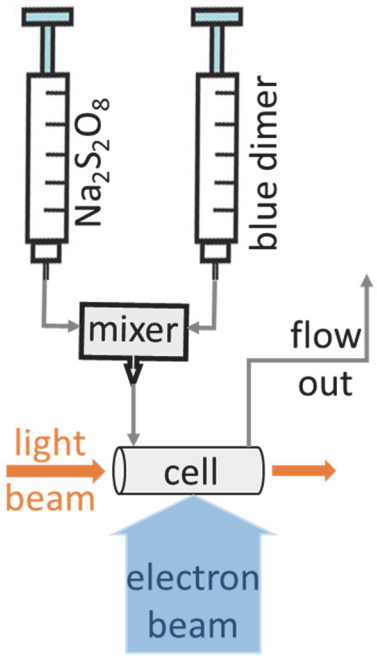

Figure S1. Experimental setup for performing pulse radiolysis with flow pre-mixing. Two Ar-purged buffered (2 mM borate, pH 9.2 plus 10 mM *tert*-butyl alcohol) solutions, one containing 20 μM **{3,3}** and the other containing 4 mM $S_2O_8^{2-}$, are flow-mixed and passed into an optical flow cell using a remotely-controlled syringe pump. The electron pulse and optical kinetics detection are timed to occur while the solutions are still flowing.

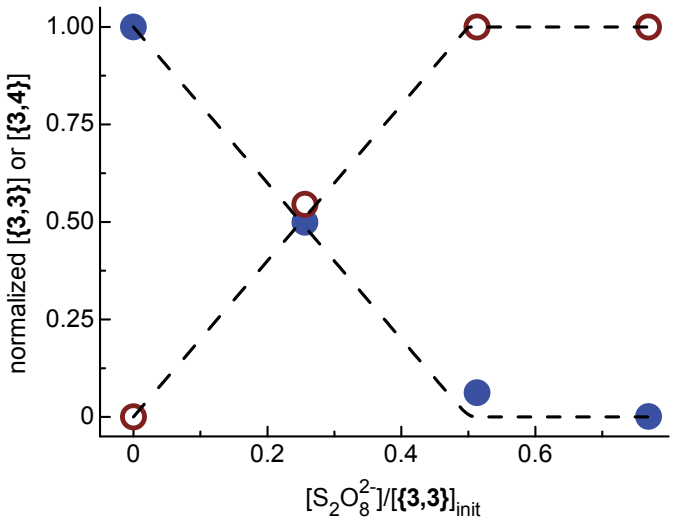

Figure S2. Stoichiometry of the **{3,3}** + $S_2O_8^{2-}$ reaction. Incremental additions of $K_2S_2O_8$ were made to ~20 μM **{3,3}** in 4 mM sodium borate, pH 9.2, at ambient temperature. Concentrations of **{3,3}** and **{3,4}** in product solutions were determined at their visible absorption maxima; data are normalized to the initial amount of **{3,3}** present (denoted $[\mathbf{\{3,3\}}]_0$). Closed symbols: **{3,3}**; open symbols: **{3,4}**. The dashed lines show the theoretical results for 2-to-1 consumption of **{3,3}** by $S_2O_8^{2-}$.

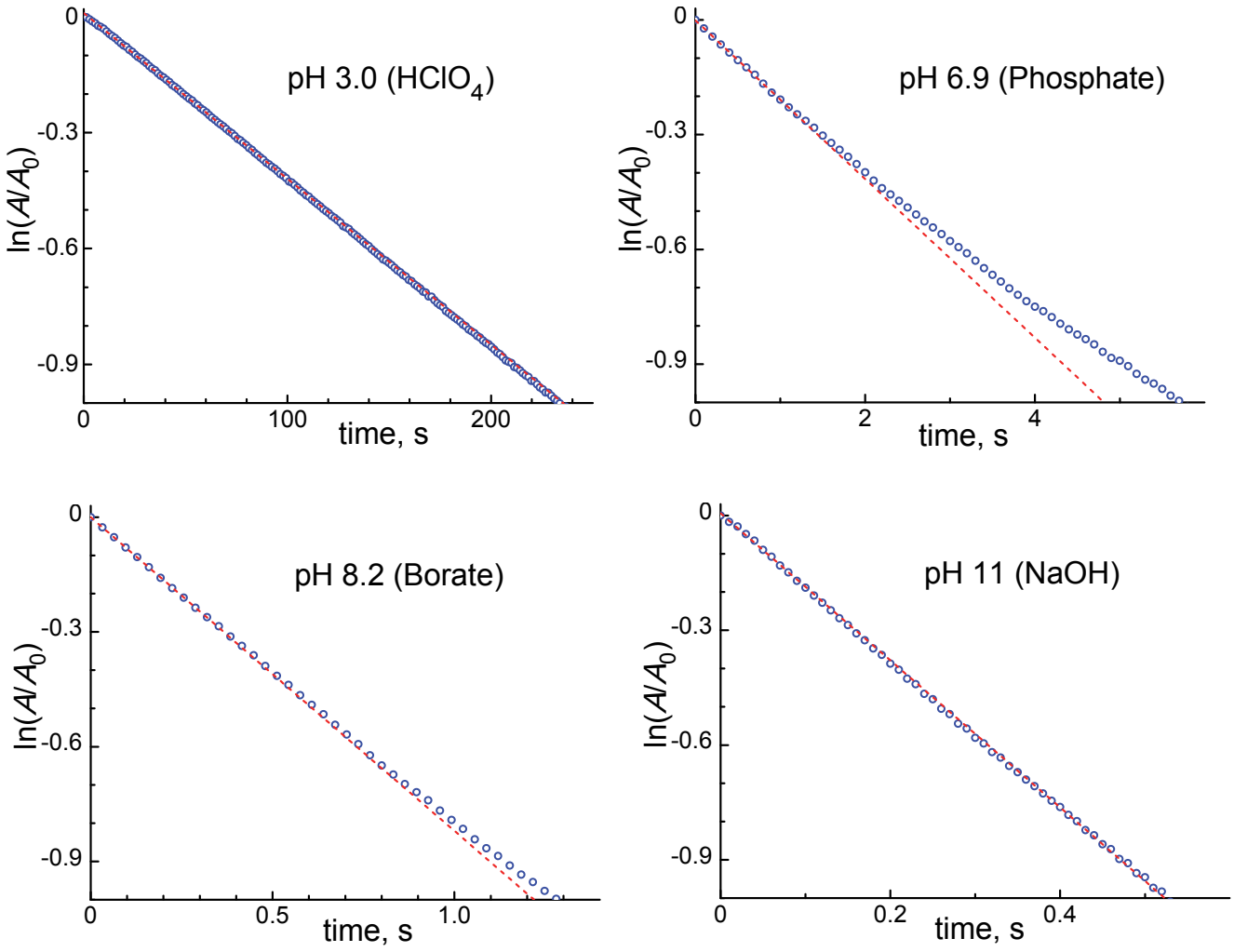

Figure S3. Semilogarithmic representation of normalized kinetic traces obtained from the decay of **{3,3}** absorption at 624 nm at various medium pH and 25 °C. Conditions: $[\mathbf{\{3,3\}}]_0 \approx 20$ μM, $[S_2O_8^{2-}] = 10$ mM, constant ionic strength of 40 mM. Experimental data points are shown in blue. Red dashed lines give linear fits of the initial portion of the kinetics (~20 % of shown timescale). As can be seen, in both alkaline and acidic media with $S_2O_8^{2-}$ in excess, **{3,3}** decay kinetics are rigorously exponential, but significant deviations from exponentiality are observed in neutral media. Additional studies indicated that this effect is not caused by anation of the complex ion; specifically, $t_{½}$ values measured for first-order substitution of 5-40 mM phosphate at pH 7.2 were $(3\text{-}0.9)\times10^3$ s, far too slow to interfere with oxidation initiated by flow-mixing solutions of unbuffered **{3,3}** and phosphate-buffered $K_2S_2O_8$, and nearly identical deviations were observed when the cationic buffer, tris-hydroxymethylaminomethane, was substituted for phosphate. Kinetic modeling indicates that comproportionation reactions also do not limit the overall reaction dynamics under these conditions. Similar kinetic effects have been noted in the reaction of $Os(bpy)_3^{2+}$ with peroxydisulfate,[3] and presumably involve side reactions or deep oxidation[4] of the complexes by $SO_4^{\bullet-}$.

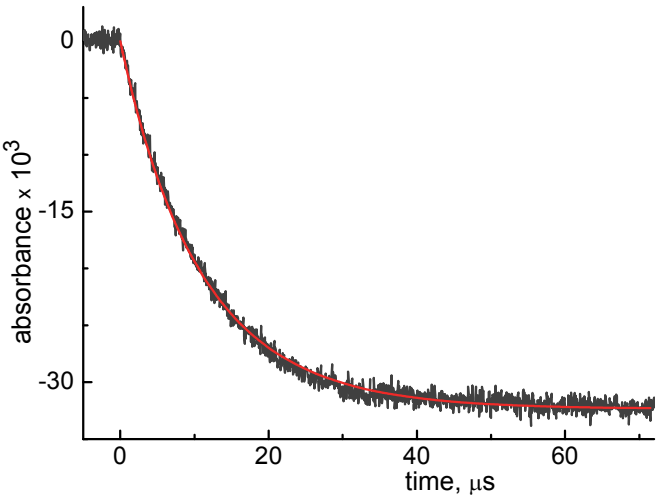

Figure S4. Typical kinetic trace recorded at 624 nm corresponding to the **{3,3}** + $(CH_3)_2$•COH reaction in an N_2O-saturated solution also containing 50 mM 2-PrOH, 20.5 μM **{3,3}**, and 2 mM NaOH. An 80 ns radiation pulse was applied to produce 0.34 μM of primary water radiolysis radicals per unit *G*-value. Under these conditions all radicals from water radiolysis

$$H_2O \text{ } \wedge\!\vee\!\wedge\!\rightarrow e_{aq}^-(2.7), OH^\bullet (2.8), H^\bullet(0.55)$$

(*G*-values are shown in parentheses) are converted into the alcohol radicals on a sub-microsecond time scale through the following rapid reactions[5-8]

$$N_2O + e_{aq}^- (+H_2O) \rightarrow N_2 + OH^- + OH^\bullet \qquad k = 9.1\times10^9 \text{ M}^{-1} \text{ s}^{-1}$$

$$(CH_3)_2CHOH + OH^\bullet \rightarrow \sim0.9(CH_3)_2{}^\bullet COH + \sim0.1{}^\bullet CH_2(CH_3)CHOH + H_2O \qquad k = 1.9\times10^9 \text{ M}^{-1} \text{ s}^{-1}$$

$$(CH_3)_2CHOH + H^\bullet \rightarrow (CH_3)_2{}^\bullet COH + H_2 \qquad k = 7.5\times10^7 \text{ M}^{-1} \text{ s}^{-1}$$

The β-carbon $^\bullet CH_2(CH_3)CHOH$ radical is not reducing. It is expected to react with the coordination complex as sluggishly as the *tert*-butanol radical ($^\bullet CH_2C(CH_3)_2OH$) and should not interfere with the dynamics of the reactions of **{3,3}** with the strongly reducing α-carbon $(CH_3)_2{}^\bullet COH$ radical. This reaction

$$(CH_3)_2{}^\bullet COH + \textbf{\{3,3\}} \rightarrow (CH_3)_2CO + H^+ + \textbf{\{2,3\}} \qquad k_{ar2}$$

and the radical-radical recombination

$$(CH_3)_2{}^\bullet COH + (CH_3)_2{}^\bullet COH \text{ (or } {}^\bullet CH_2(CH_3)CHOH) \rightarrow \text{products} \qquad k_{rec}$$

are the only processes that occur on the observational time scale. With the k_{rec} fixed at 5.8×10^8 M^{-1} s^{-1} (average of the literature data[9-13]), the k_{ar2} value was fitted to the kinetic data through numerical integration of the last two reactions, and the fit is shown by the red line in the figure. Statistical analysis of the so-obtained k_{ar2} from several kinetic traces recorded at various radiation doses yielded $k_{ar2} = (5.1 \pm 0.3)\times10^9$ M^{-1} s^{-1}.

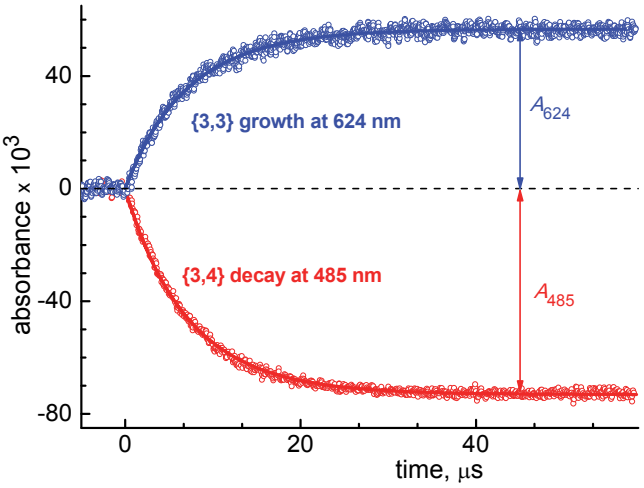

Figure S5. Typical kinetic traces of **{3,4}** decay (red) and **{3,3}** formation (blue) recorded at 485 nm and 624 nm, respectively, corresponding to the **{3,4}** to **{3,3}** conversion in an N_2O-saturated solution also containing 50 mM 2-PrOH, 20 μM **{3,4}**, ~2.5 μM $S_2O_8^{2-}$, and 3 mM NaOH. A 100 ns radiation pulse was applied that produced 0.425 μM of primary water radiolysis radicals per unit *G*-value. Under these conditions all radicals from water radiolysis are converted into the alcohol radicals on a sub-microsecond time scale as described in the caption to Figure S4. Reaction of **{3,4}** with the strongly reducing α-carbon $(CH_3)_2{}^{\bullet}COH$ radical

$$(CH_3)_2{}^{\bullet}COH + \mathbf{\{3,4\}} \rightarrow (CH_3)_2CO + H^+ + \mathbf{\{3,3\}} \qquad k_{ar1}$$

and the radical-radical recombination

$$(CH_3)_2{}^{\bullet}COH + (CH_3)_2{}^{\bullet}COH \text{ (or } {}^{\bullet}CH_2(CH_3)CHOH) \rightarrow \text{products} \qquad k_{rec}$$

are the only processes that occur on the observational time scale. With the k_{rec} fixed at 5.8×10^8 M^{-1} s^{-1} (average of the literature data[9-13]), the k_{ar1} value was fitted to the kinetic data through numerical integration of these two reactions, and the fits shown by the solid lines in the figure yielded the same $k_{ar1} = 7.2\times10^9$ M^{-1} s^{-1}. The signal amplitude ratio $A_{485}/A_{624} = 1.3$ matches the **{3,4}** – **{3,3}** difference spectrum at this pH, as expected for the k_{ar1} reaction being the only reaction involving the blue dimer.

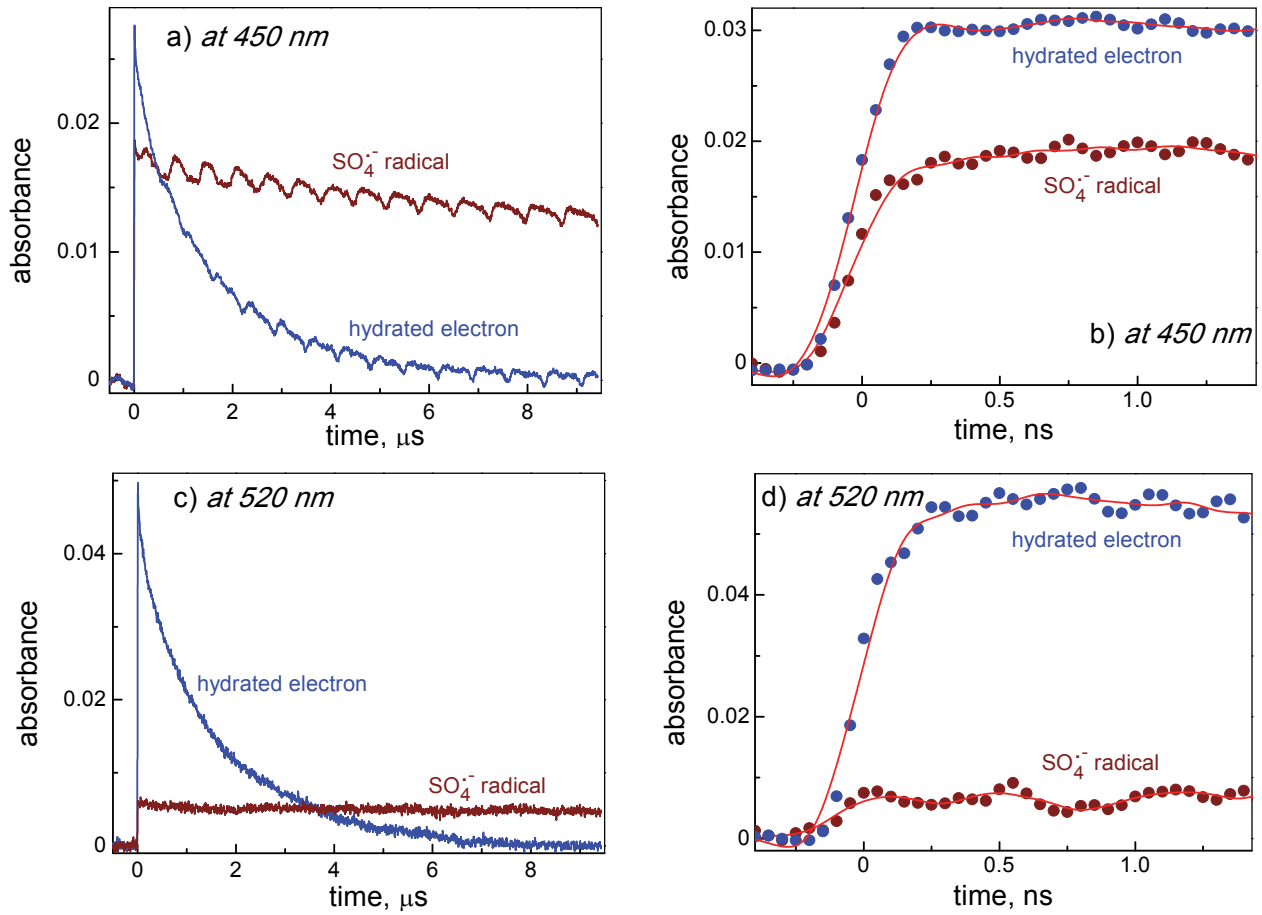

Figure S6. Kinetics of the $SO_4^{\bullet-}$ radical (wine) and hydrated electron (blue) obtained by picosecond pulse radiolysis of Ar-purged 2 M solution of $K_2S_2O_8$ and neat water, respectively. Traces recorded at 450 nm ($SO_4^{\bullet-}$ absorption maximum)[14] on microsecond (a) and sub-nanosecond (b) time scales, and at 520 nm (away from $SO_4^{\bullet-}$ absorption maximum) on microsecond (c) and sub-nanosecond (d) time scales. The red lines serve only to smooth the data and have no analytical significance. A ~30 ps radiation pulse was applied to all samples. In the absence of $S_2O_8^{2-}$, the only observable radiolysis product is the hydrated electron that absorbs more strongly at 520 nm than at 450 nm and decays with a ~1 μs half-life. With 2 M $Na_2S_2O_8$, the electrons are quantitatively captured by $S_2O_8^{2-}$ within ~0.05 ns,[15] and the observed absorption that persists well into the microsecond time scale is attributable to the $SO_4^{\bullet-}$ radical generated through reductive decomposition of $S_2O_8^{2-}$

$$S_2O_8^{2-} + e^- \rightarrow \{S_2O_8^{\bullet 3-}\} \rightarrow SO_4^{2-} + SO_4^{\bullet-}$$

The rise of the hydrated electron signal in panels (b) and (d) represents the electronic rise time of the detection system. The same rise time for the electron and $SO_4^{\bullet-}$, which is clearly seen in panel (b), indicates that, even if the $S_2O_8^{\bullet 3-}$ radical exists as the bound thermally equilibrated species, its lifetime does not exceed 0.5 ns.

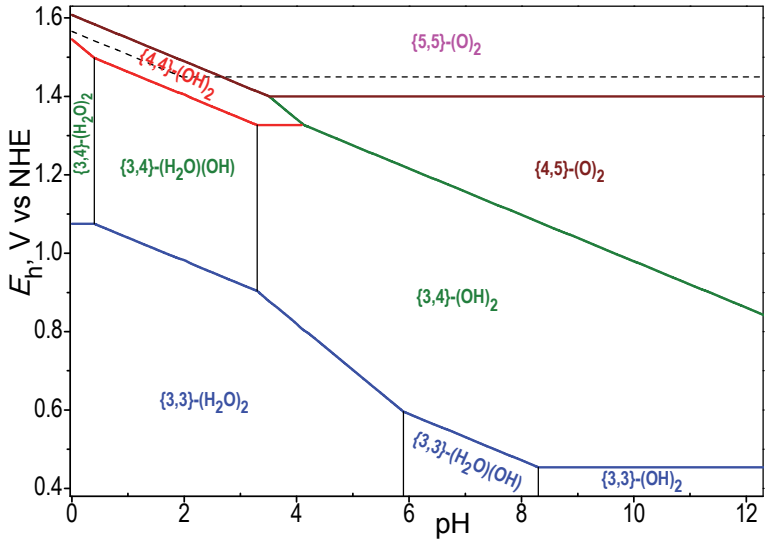

Figure S7. E_h–pH predominance diagram for blue dimer species computed using raw literature data uncorrected for ionic strength that are summarized in Tables S1 and S2. The dashed line corresponds to the one-electron reduction potential of peroxydisulfate: $E^0(S_2O_8^{2-}/SO_4^{\bullet-},SO_4^{2-})$ = 1.45 V and $pK_a(HSO_4^-)$ = 1.96.

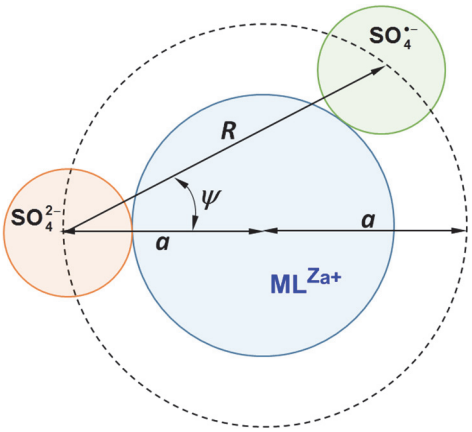

Figure S8. An instantaneous configuration of an ion triple formed by a ML^{z_a+} cation, SO_4^{2-} anion (Z_b = -2), and $SO_4^{\bullet-}$ radical (Z_c = -1). In the case of **{3,4}** cation, Z_a = 3-5, depending on the protonation state. The ionic radii are taken as r_a = 5.2 Å and $r_b = r_c$ = 1.5 Å (see page 1), which gives the center-to-center anion-cation separation between $a = r_a + r_b$ = 6.7 Å and $a + \delta r$ = 7.7 Å. The ion triple formation constant (at μ = 0) is computed in three steps. In step 1, the $SO_4^{\bullet-}$ radical is not present and the ion pairing constant between **{3,4}** and SO_4^{2-} is evaluated in the usual way (see main text eqs. 6 and 7)

$$K' = \frac{[\{\mathbf{3,4}\}\cdots SO_4^{2-}]_{IP}}{[\{\mathbf{3,4}\}][SO_4^{2-}]} = \frac{4\pi L a^2 \delta r}{1000} exp\left(-\frac{Z_a Z_b e^2}{DakT}\right) \quad \text{(S1)}$$

Here, L is the Avogadro number, e is the electron charge, D is the bulk dielectric constant of water, and the other symbols have their usual meanings. In step 2, the $SO_4^{\bullet-}$ radical is brought in and allowed to reside anywhere between a and $a + \delta r$ from the center of **{3,4}** except the space already occupied by SO_4^{2-}; that is, the shortest center-to-center distance between SO_4^{2-} and $SO_4^{\bullet-}$ is $R_{min} = 2a \times cos(\psi_{max}) = r_b + r_c$ = 3 Å and the maximum angle is ψ_{max} = 77 degrees. The equilibrium constant for $SO_4^{\bullet-}$ addition

$$K'' = \frac{[SO_4^{\bullet-}\cdots\{\mathbf{3,4}\}\cdots SO_4^{2-}]_{IT}}{[\{\mathbf{3,4}\}\cdots SO_4^{2-}]_{IP}[SO_4^{\bullet-}]}$$

can be readily obtained from the above model

$$K'' = \frac{8\pi L a^2 \delta r}{1000} exp\left(-\frac{Z_A Z_C e^2}{DakT}\right) \int_0^{\psi_{max}} exp\left(-\frac{Z_b Z_c e^2}{D(2a\,cos\,\psi)kT}\right) cos\,\psi sin\,\psi d\psi \quad \text{(S2)}$$

and evaluated through numerical integration. Finally, the ion triple formation constant is computed by combining eqs. S1 and S2

$$K_{IT} = \frac{[SO_4^{\bullet-}\cdots\{\mathbf{3,4}\}\cdots SO_4^{2-}]_{IT}}{[\{\mathbf{3,4}\}][SO_4^{2-}][SO_4^{\bullet-}]} = K'K''$$

The entropy of ion tripling can be evaluated from

$$\Delta_{IT}S = -R\frac{\partial(TlnK_{IT})}{\partial T}$$

taking into account the temperature dependence of D.

Table S1. pK_a of blue dimer species.

Entry	Species	Charge	Observed[a]		Corrected[b]
			pK_a	μ, M	pK_a^0 ($\mu \to 0$)
pK_{a1}	H_2O-**{3,3}**-OH_2	+4	5.9	0.1[c]	5.1
pK_{a2}	HO-**{3,3}**-OH_2	+3	8.3	0.3[d]	7.6
pK_{a3}	H_2O-**{3,4}**-OH_2	+5	0.4	0.4[e]	-0.7
pK_{a4}	HO-**{3,4}**-OH_2	+4	3.3	0.1[f]	2.6

[a]From Gilbert et. al.;[2] although ionic strengths have not been precisely specified, their approximate values could be deduced from the general experimental description; [b]Computed using Davies activity coefficient corrections $log\gamma_i = -0.509Z_i^2\left(\frac{\sqrt{\mu}}{1+\sqrt{\mu}} + 0.3\mu\right)$ and $pK_a^0 = pK_a^{obs} + log\gamma_{acid} - log\gamma_{base} - log\gamma_{H^+}$, with the last term omitted for $pK_a^{obs} > 3$; note the relatively large corrections arising from the large charges of the species involved; [c]In 0.1 M phosphate buffer at pH 6; [d]In 0.1 M phosphate buffer at pH 8; [e]In 0.4 M triflic acid; [f]In 0.1 M triflate.

Table S2. Reduction potentials of blue dimer species vs. NHE.

Entry	Half-cell reaction	Observed E', V (μ, M)	Corrected[a] E^0 ($\mu\rightarrow0$), V
Primary data			
E_1	$[H_2O\text{-}\{\mathbf{3,4}\}\text{-}OH_2]^{5+} + e^- = [H_2O\text{-}\{\mathbf{3,3}\}\text{-}OH_2]^{4+}$	1.07[b] (0.5)	1.16[c]
E_2	$[HO\text{-}\{\mathbf{4,4}\}\text{-}OH]^{4+} + e^- + 2H^+ = [H_2O\text{-}\{\mathbf{3,4}\}\text{-}OH_2]^{5+}$	1.53[b] (0.5)	1.49[d]
E_3	$[O\text{-}\{\mathbf{5,5}\}\text{-}O]^{4+} + 2e^- + 2H^+ = [HO\text{-}\{\mathbf{4,4}\}\text{-}OH]^{4+}$	1.59[b] (0.5)	1.62[e]
E_4	$[O\text{-}\{\mathbf{5,5}\}\text{-}O]^{4+} + e^- = [O\text{-}\{\mathbf{4,5}\}\text{-}O]^{3+}$	1.41[f] (0.18)	1.46[g]
Derived one-electron potentials[h]			
E_5	$[HO\text{-}\{\mathbf{3,4}\}\text{-}OH]^{3+} + e^- = [HO\text{-}\{\mathbf{3,3}\}\text{-}OH]^{2+}$	0.46	0.51
E_6	$[HO\text{-}\{\mathbf{3,4}\}\text{-}OH]^{3+} + e^- + H^+ = [H_2O\text{-}\{\mathbf{3,3}\}\text{-}OH]^{3+}$	0.96	0.96
E_7	$[HO\text{-}\{\mathbf{3,4}\}\text{-}OH]^{3+} + e^- + 2H^+ = [H_2O\text{-}\{\mathbf{3,3}\}\text{-}OH_2]^{4+}$	1.30	1.27
E_8	$[H_2O\text{-}\{\mathbf{3,4}\}\text{-}OH]^{4+} + e^- + H^+ = [H_2O\text{-}\{\mathbf{3,3}\}\text{-}OH_2]^{4+}$	1.11	1.12
E_9	$[H_2O\text{-}\{\mathbf{3,4}\}\text{-}OH]^{4+} + e^- = [H_2O\text{-}\{\mathbf{3,3}\}\text{-}OH]^{3+}$	0.76	0.81
E_{10}	$[HO\text{-}\{\mathbf{4,4}\}\text{-}OH]^{4+} + e^- = [HO\text{-}\{\mathbf{3,4}\}\text{-}OH]^{3+}$	1.33	1.38
E_{11}	$[HO\text{-}\{\mathbf{4,4}\}\text{-}OH]^{4+} + e^- + H^+ = [H_2O\text{-}\{\mathbf{3,4}\}\text{-}OH]^{4+}$	1.52	1.53
E_{12}	$[O\text{-}\{\mathbf{4,5}\}\text{-}O]^{3+} + e^- + 2H^+ = [HO\text{-}\{\mathbf{4,4}\}\text{-}OH]^{4+}$	1.82	1.77

[a]Computed using Davies activity coefficient corrections $log\gamma_i = -0.509Z_i^2\left(\frac{\sqrt{\mu}}{1+\sqrt{\mu}} + 0.3\mu\right)$; [b]In 0.5 M triflic acid;[16] [c]Computed from $E^0 = E' - 0.059\left(logF + log\frac{\gamma_{\{3,4\}}}{\gamma_{\{3,3\}}}\right)$, where $F = \frac{[H^+]}{[H^+]+[K_{a3}^{obs}]}$ is the fraction of fully-protonated **{3,4}** under conditions for measuring E'; [d]Computed from $E^0 = E' + 0.059\left(logF + log\frac{\gamma_{\{3,4\}}}{\gamma_{\{4,4\}}} - 2log(\gamma_{H^+}[H^+])\right)$; [e]Computed from $E^0 = E' - 0.059\left(\frac{1}{2}log\frac{\gamma_{\{5,5\}}}{\gamma_{\{4,4\}}} + log(\gamma_{H^+}[H^+])\right)$; [f]In 0.1 M phosphate buffer at pH 7;[2] [g]Computed from $E^0 = E' - 0.059log\frac{\gamma_{\{5,5\}}}{\gamma_{\{4,5\}}}$; [h]Derived using corresponding μ-corrected and uncorrected $E_1 - E_4$ from this table and pK_a from Table S1.

Table S3. Data for correlating k_{et} with $\Delta G^{0'}$. In blue are values projected from the data in Fig. 11 and Table S2.

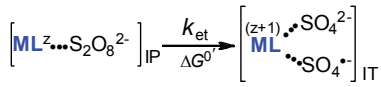

Entry	ML^z	Z	r_z[a]	Observed[a]		Evaluated[a] ($\mu \rightarrow 0$)			Corrected[a] ($\mu \rightarrow 0$)		
				$2K_{IP}k_{et}$ (μ)	E^0	K_{IP}[b]	K_{IT}[c]	$-\Delta G^{0}$[,d]	$2K_{IP}k_{et}$[,b]	$log(k_{et})$	$-\Delta G^{0'}$[,e]
Blue dimer species (this work)											
1	HO-**{3,3}**-OH	+2	5.2	200 (40)	0.51	20	290	0.94	720	1.26	1.01
2	HO-**{3,3}**-OH_2	+3		15 (40)	0.81	140	6.5×10^3	0.64	100	-0.44	0.74
3	H_2O-**{3,3}**-OH_2	+4		0.40 (40)	1.16	1.0×10^3	1.5×10^5	0.29	5.2	-2.59	0.42
4	HO-**{3,4}**-OH	+3		**2.4×10^{-3} (30)**	**1.38**	**140**	**6.5×10^3**	**0.07**	**0.017**	**-4.23**	**0.17**
5	O-**{4,5}**-O	+3		**8.7×10^{-4} (30)**	**1.46**	**140**	**6.5×10^3**	**-0.01**	**0.005**	**-4.76**	**0.09**
Mononuclear polypyridine- and o-phenanthroline-based complexes (literature data)											
6	$Ru(bpy)_3$	+2	4.8[f]	0.011(300)[17]	1.26[18]	22	370	0.19	0.11	-2.60	0.26
				9.0×10^{-3} (0)[19]					0.009	-3.69	
7	$Os(bpy)_3$	+2	4.8[f]	49 (0)[19]	0.82[18]	22	370	0.63	49	0.046	0.70
8	$Fe(bpy)_3$	+2	4.8[f]	0.55 (0)[19]	1.05[18]	22	370	0.40	0.55	-1.90	0.47
				0.41 (6)[20]					0.76	-1.76	
				0.40 (0)[21]					0.40	-2.04	
9	Fe(4,4′-Me_2-bpy)$_3$	+2	5.0[g]	6.7 (0)[19]	0.94[19]	21	320	0.51	6.7	-0.79	0.58
				6.0 (6)[20]					11.1	-0.57	
				5.8 (0)[21]					5.8	-0.86	
10	$Fe(tpy)_2$	+2	4.8[h]	0.51 (6)[20]	1.05[18]	22	370	0.63	0.95	-1.67	0.47
11	$Fe(phen)_3$	+2	5.0[i]	0.11 (6)[20]	1.15[j]	21	320	0.30	0.20	-2.32	0.37
				0.30 (0)[19]					0.30	-2.14	
				0.21 (0)[21]					0.21	-2.30	
12	Fe(5-Cl-phen)$_3$	+2	5.0[k]	0.042 (6)[20]	1.15[l]	21	320	0.30	0.078	-2.73	0.37
				0.272 (0)[21]					0.272	-2.18	
13	Fe(5-Me-phen)$_3$	+2	5.0[k]	0.078 (6)[20]	1.15[19]	21	320	0.30	0.15	-2.46	0.37
				0.11 (0)[19]					0.11	-2.58	
				0.086 (0)[21]					0.086	-2.68	

Entry	ML^z	Z	r_z[a]	Observed[a]		Evaluated[a] ($\mu \rightarrow 0$)			Corrected[a] ($\mu \rightarrow 0$)		
				$2K_{IP}k_{et}$ (μ)	E^0	K_{IP}[b]	K_{IT}[c]	$-\Delta G^{0}$[,d]	$2K_{IP}k_{et}$[,b]	$log(k_{et})$	$-\Delta G^{0'}$[,e]
Mononuclear $(NH_3)_5Ru^{II}L$ complexes (literature data)											
14	$(NH_3)_5Ru(pz)^m$	+2	3.8[22]	7.2×10^3 (100)[22]	0.55[n]	33	920	0.90	4.6×10^4	2.85	0.99
15	$(NH_3)_5Ru(Me\text{-}pz)^m$	+3	3.9[22]	190 (100)[22]	0.91[p]	350	4.0×10^4	0.54	3.1×10^3	0.64	0.66
16	$(NH_3)_5Ru(bpa)^m$	+2	3.9[q]	2.0×10^5 (100)[23]	0.33[r]	32	830	1.13	1.3×10^6	4.31	1.21
Pyrazine-bridged binuclear pentammine complexes (literature data)											
17	$(NH_3)_5Ru\text{-}pz\text{-}Ru(NH_3)_5^m$	+5	4.7[22]	2.6×10^4 (100)[22]	0.83[s]	1.3×10^4	1.0×10^7	0.62	2.1×10^6	1.91	0.79
18	$(NH_3)_5Ru\text{-}pz\text{-}Rh(NH_3)_5^m$	+5	4.7[22]	4.2×10^4 (100)[22]	0.78[t]	1.3×10^4	1.0×10^7	0.67	3.4×10^6	2.12	0.84

[a]Units: radius of ML^Z in Å, $2K_{IP}k_{et}$ in M^{-1} s^{-1}, μ in mM, $E^0(ML^{(z+1)}/ML^z)$ in V vs. NHE, ΔG^0 and $\Delta G^{0'}$ in eV/molecule, K_{IP} in M^{-1}, and K_{IT} in M^{-2}; [b]Computed using eq. 4 and 6-7 (main text) and $r_0 = r_z + 1.9$ Å; [c]Computed as described in Fig. S8; [d]Evaluated from $E^0(ML^{(z+1)}/ML^z)$ and $E^0(S_2O_8^{2-}/SO_4^{\bullet-},SO_4^{2-}) = 1.45$ V; [e]Computed using eq. 20 (main text); [f]Taken to be equal to r_z for $Co(bpy)_3$;[24] [g]Increased by 0.2 Å compared to $Fe(bpy)_3$; [h]Taken the same as for $Fe(bpy)_3$; [i]Derived from conductivity;[24] [j]HCP on the web: *CRC Handbook of Chemistry and Physics,* 95th ed, 2014-2015, http://www.hbcpnetbase.com (Accessed December 18, 2014); [k]Taken to be the same as for $Fe(phen)_3$; [l]Corrected from 1.12 V determined in 1 M H_2SO_4;[25] [m]pz = pyrazine, Me-pz = N-methylpyrazinium, bpa = 1,2-bis(4-pyridyl)ethane; [n]Corrected from 0.52 V at $\mu = 0.1$ M;[26] [p]Corrected from 0.87 V at $\mu = 0.1$ M;[26] [q]Taken to be equal to r_z for $(NH_3)_5Ru(Me\text{-}pz)$; [r]Corrected from 0.293 V at $\mu = 0.1$ M;[23] [s]Corrected from 0.76 V at $\mu = 0.1$ M;[27] [t]Corrected from 0.71 V at $\mu = 0.1$ M.[27]

Table S4. Activation parameters for complex ion oxidations by $S_2O_8^{2-}$ derived from temperature dependencies of the apparent bimolecular rate constant $k_{app} = 2K_{IP}k_{et}$.

Entry	ML^z	Z	A_{app} $M^{-1}s^{-1}$	$log_{10}(A_{app})$	$-\Delta S^{\#}_{app}$ eu	E_a, kcal/mol	$\Delta H^{\#}_{app}$ kcal/mol
Blue dimer (this work)							
1	HO-**{3,3}**-OH	+2	4.5×10^8	8.65	20.9	8.11	7.52
Mononuclear polypyridine- and o-phenanthroline-based complexes (literature data)[a]							
2	$Ru(bpy)_3$	+2	5.0×10^8 [19]	8.70	20.7	14.6 [19]	14.0
3	$Os(bpy)_3$	+2	2.8×10^8 [3]	8.45	21.9	9.4 [3]	8.81
4	$Fe(bpy)_3$	+2	5.7×10^8 [19]	8.76	20.5	12.4 [19]	11.8
			1.0×10^7	7 [20]	28.5	10.3 [20]	9.71
			2.5×10^7	7.39	26.7 [21]	10.6	10 [21]
5	$Fe(4,4'\text{-}Me_2\text{-}bpy)_3$	+2	1.0×10^6	6 [20]	33.1	6.6 [20]	6.01
			7.6×10^6	6.85	29.2 [21]	8.23	7.64 [21]
6	$Fe(5,5'\text{-}Me_2\text{-}bpy)_3$	+2	1.0×10^6	6 [20]	33.1	7.8 [20]	7.21
7	$Fe(tpy)_2$	+2	1.0×10^8	8 [20]	23.9	10.7 [20]	10.1
8	$Fe(phen)_3$	+2	1.0×10^9	9 [20]	19.3	13.5 [20]	12.9
			1.5×10^9 [19]	9.18	18.5	13.3 [19]	12.7
			3.4×10^8	8.53	21.5 [21]	12.7	12.1 [21]
9	$Fe(5\text{-}Me\text{-}phen)_3$	+2	1.0×10^8	8 [20]	23.9	11.9 [20]	11.3
			1.6×10^8 [19]	8.20	23.0	12.6 [19]	12.0
			6.8×10^7	7.83	24.7 [21]	12.8	12.2 [21]
10	$Fe(5,6\text{-}Me_2\text{-}phen)_3$	+2	1.0×10^8	8 [20]	23.9	13.3 [20]	12.7
11	$Fe(4,7\text{-}Me_2\text{-}phen)_3$	+2	1.0×10^5	5 [20]	37.7	6.9 [20]	6.31
12	$Fe(3,5,6,8\text{-}Me_4\text{-}phen)_3$	+2	1.0×10^6	6 [20]	33.1	9.1 [20]	8.51
13	$Fe(5\text{-}Cl\text{-}phen)_3$	+2	1.0×10^{14}	14 [20]	-3.53	20.7 [20]	20.1
			4.1×10^{11}	11.6	7.4 [21]	17.9	17.3 [21]
Average[b]			**5.2×10^{12}**	**8.1**	**23.4**	**11.8**	**11.2**

[a]References are shown next to the actually reported data; [b]Excluding the first entry.

References

(1) Allan, D. R. Sodium Peroxodisulfate. *Acta Cryst. E* **2006**, *62*, i44-i46.

(2) Gilbert, J. A.; Eggleston, D. S.; Murphy, W. R.; Geselowitz, D. A.; Gersten, S. W.; Hodgson, D. J.; Meyer, T. J. Structure and Redox Properties of the Water-Oxidation Catalyst $[(bpy)_2(OH_2)RuORu(OH_2)(bpy)_2]^{4+}$. *J. Am. Chem. Soc.* **1985**, *107*, 3855-3864.

(3) Irvine, D. H. The Oxidation of the Trisdipyridylosmium(II) Ion by the Peroxydisulphate Ion in Aqueous Solution. *J. Chem. Soc.* **1958**, 2166-2170.

(4) Ghosh, P. K.; Brunschwig, B. S.; Chou, M.; Creutz, C.; Sutin, N. Thermal and Light-Induced Reduction of $Ru(bpy)_3^{3+}$ in Aqueous Solution. *J. Am. Chem. Soc.* **1984**, *106*, 4772-4783.

(5) Buxton, G. V.; Greenstock, C. L.; Helman, W. P.; Ross, A. B. Critical Review of Rate Constants for Reactions of Hydrated Electrons, Hydrogen Atoms and Hydroxyl Radicals ($^{\cdot}OH/^{\cdot}O^-$) in Aqueous Solution. *J. Phys. Chem. Ref. Data* **1988**, *17*, 513-886.

(6) Asmus, K.-D.; Möckel, H.; Henglein, A. Pulse Radiolytic Study of the Site of Hydroxyl Radical Attack on Aliphatic Alcohols in Aqueous Solution. *J. Phys. Chem.* **1973**, *77*, 1218-1221.

(7) Mulazzani, Q. G.; D'Angelantonio, M.; Venturi, M.; Hoffman, M. Z.; Rodgers, M. A. J. Interaction of Formate and Oxalate Ions with Radiation-Generated Radicals in Aqueous Solution. Methylviologen as a Mechanistic Probe. *J. Phys. Chem.* **1986**, *90*, 5347-5352.

(8) Lymar, S. V.; Poskrebyshev, G. A. Rate of $ON\text{-}OO^-$ bond homolysis and the Gibbs energy of formation of peroxynitrite. *J. Phys. Chem. A* **2003**, *107*, 7991-7996.

(9) Simic, M.; Neta, P.; Hayon, E. Pulse Radiolysis of Alcohols in Aqueous Solution. *J. Phys. Chem.* **1969**, *73*, 3794-3800.

(10) Rabani, J.; Mulac, W. A.; Matheson, M. S. Pulse Radiolysis Studies of Zn^+ Reactions. *J. Phys. Chem.* **1977**, *81*, 99-104.

(11) Lehni, M.; Fischer, H. Effects of Diffusion on the Self-Termination Kinetics of Isopropylol Radicals in Solution. *Int. J. Chem. Kinet.* **1984**, *15*, 733-757.

(12) Wu, L.-M.; Fischer, H. Self- and Cross-Termination Rate Constants for the Isopropylol Radical and Its Anion in Aqueous Solution. *Int. J. Chem. Kinet.* **1984**, *16*, 1111-1115.

(13) Shastri, L. V.; Mittal, L. J.; Mittal, J. P. Radiation Chemical Separation of Europium from Aqueous Lanthanide Mixtures. *Radiat. Phys. Chem.* **1986**, *28*, 359-361.

(14) Hug, G. *Optical Spectra of Nonmetallic Inorganic Transients in Aqueous Solution*, US Department of Commerce/Natl. Bureau of Standards, 1981.

(15) Hunt, J. W. Early Events in Radiation Chemistry. In *Advances in Radiation Chemistry*; Burton, M., Magee, J. L., Eds.; Wiley: New York, 1976; Vol. 5, p 185-315.

(16) Yamada, H.; Hurst, J. K. Resonance Raman, Optical Spectroscopic, and EPR Characterization of the Higher Oxidation States of the Water Oxidation Catalyst, *cis,cis*-$[(bpy)_2Ru(OH_2)]_2O^{4+}$. *J. Am. Chem. Soc.* **2000**, *122*, 5303-5311.

(17) Lewandowska-Andralojc, A.; Polyansky, D. E. Mechanism of the Quenching of the Tris(bipyridine)ruthenium(II) Emission by Persulfate: Implications for Photoinduced Oxidation Reactions. *J. Phys. Chem. A* **2013**, *117*, 10311-10319.

(18) Creutz, C.; Chou, M.; Netzel, T. L.; Okumura, M.; Sutin, N. Lifetimes, Spectra, and Quenching of the Excited States of Polypyridine Complexes of Iron(II), Ruthenium(II), and Osmium(II). *J. Am. Chem. Soc.* **1980**, *102*, 1309-1319.

(19) Irvine, D. H. The Kinetics of the Oxidation of Some Bipyridyl and Phenanthroline Complex Ions by the Peroxydisulphate Ion in Aqueous Solution. *J. Chem. Soc.* **1959**, 2977-2981.

(20) Burgess, J.; Prince, R. H. Peroxydisulphate Oxidation of Iron(II) Complexes of Substituted 1,10-Phenanthrolines and Related Compounds. *J. Chem. Soc. A* **1966**, 1772-1775.

(21) Raman, S.; Brubaker Jr, C. H. The Kinetics of the Oxidation of Substituted 2,2′-Bipyridine and 1,10-Phenanthroline Complexes of Iron(II) with Peroxydisulfate Ion. *J. Inorg. Nucl. Chem.* **1969**, *31*, 1091-1099.

(22) Fürholz, U.; Haim, A. Kinetics and Mechanisms of the Reactions of Mononuclear and Binuclear Ruthenium(II) Ammine Complexes with Peroxydisulfate. *Inorg. Chem.* **1987**, *26*, 3243-3248.

(23) Olabe, J. A.; Haim, A. An Example of Intramolecular Electron-Transfer Assistance in a Bimolecular Redox Reaction: Peroxydisulfate Oxidation of (μ-1,2-Bis(4-pyridyl)ethane)pentaammineruthenium(III) Pentacyanoferrate(II) via Its Electronic Isomer. *Inorg. Chem.* **1989**, *28*, 3277-3278.

(24) Yokoyama, H.; Shinozaki, K.; Hattori, S.; Miyazaki, F.; Goto, M. Conductometric Study of Hydrophobic Properties of Tris(1,10-Phenanthroline) and Tris(2,2′-Bipyridine) Complexes. *J. Mol. Liq.* **1995**, *65–66*, 357-360.

(25) Brandt, W. W.; Gullstrom, D. K. Studies on Some Ferrous Complexes of Substituted 1,10-Phenanthrolines1. *J. Am. Chem. Soc.* **1952**, *74*, 3532-3535.

(26) Yeh, A.; Haim, A. Aqueous Solution Chemistry of μ-Pyrazinepentaammineruthenium(II,III) Pentacyanoferrate(II,III): Formation, Redox Reactions, and Intervalence Properties. *J. Am. Chem. Soc.* **1985**, *107*, 369-376.

(27) Creutz, C.; Taube, H. Binuclear Complexes of Ruthenium Ammines. *J. Am. Chem. Soc.* **1973**, *95*, 1086-1094.